14th IEA Heat Pump Conference
15-18 May 2023, Chicago, Illinois

Numerical evaluation of high-temperature heat pump and thermal energy storage system for industrial processes

Seon Tae Kim*, Robert Hegner, Göksel Özuylasi, Panagiotis Stathopoulos, Eberhard Nicke

Institute of Low-Carbon Industrial Processes, German Aerospace Center (DLR),
Mandauhöfe, Haus 9, Äußere Oybiner Straße 14/16, 02763, Zittau, Germany

Abstract

A numerical investigation was conducted on a high-temperature heat pump (HTHP) that can supply heat at 200°C and two types of thermal energy storage (TES) systems. The HTHP cycle employs a multistage water vapor compression process to achieve a high-temperature lift. Concrete was used as the sensible heat storage (SHS) system, while strontium bromide/water ($SrBr_2/H_2O$) was used as the working pair for the thermochemical energy storage (TCES) system. The multistage HTHP cycle was first analyzed based on an enthalpy balance with specific temperature conditions, and then the performance of both the SHS and TCES systems connected to the HTHP cycle was estimated.
The HTHP cycle achieved a COP of 4.41 with an evaporation temperature of 90°C and a condensation temperature of 160°C. During storage, 500 kW of heat was supplied at 200 °C for 8 hours. The TCES system required 45% and 68% less mass and volumetric size, respectively, in storage mode. During discharge operation, the TCES system was able to supply heat at a temperature of over 200°C under all conditions, while the SHS system had a maximum cycle out temperature of 180°C. The TCES system also had a heat output rate of ~500 kW and round-trip efficiency (RTE) of 0.82.

Selection and/or peer-review under the responsibility of the organizers of the 14th IEA Heat Pump Conference 2023.

Keywords: High-Temperature Heat Pump, Multistage Vapor Compression Cycle, Thermal Energy Storage;

1. Introduction

The global greenhouse gas (GHG) emissions have steadily increased over the past few decades. Among the various emission sectors, the industrial sector is responsible for 34.8% of global GHG emissions after reallocating to the final energy consumption sectors, and the industrial sector is becoming increasingly important [1,2].

In 2019, 120944 PJ of energy were consumed in the industrial sector, and fossil fuels accounted for over 58% (70544 PJ). Thermal energy is the dominant energy carrier in the industrial sector and each industrial sub-sector has a different main temperature level respectively [3].

Waste heat recovery is an excellent solution for improving the efficiency of existing industrial processes [4,5]. However, heat recovery at low temperatures is generally not feasible. Another efficient option for recovering waste heat from industrial processes is to use highly efficient thermal power thermodynamic engines and heat pumps. Heat pumps are widely used in domestic applications and are applied to some niche industrial processes. Electrically driven heat pumps have proven to be suitable for supplying process heat effectively; however, industrial heat pumps can deliver heat at a maximum temperature of 150°C, mainly because of component limitations [6,7]. Despite this shortcoming, there have been several research and development efforts to push the sink temperature of industrial heat pumps to 200-250°C thus extending their availability for a larger proportion of industrial processes [8,9].

* Corresponding author. Tel.: +49-3583-58545-14.
E-mail address: seon.kim@dlr.de.

Thermal energy storage (TES) systems can store heat or cold to be used later at different temperatures, places, or power is mainly used to overcome the mismatch between energy generation and demand [10]. There are three types of TES systems: sensible heat storage, latent heat storage, and thermochemical storage. Sensible heat storage (SHS) is stored by increasing or decreasing the temperature of the storage material. Latent heat storage uses the phase transition of materials, usually a solid-liquid phase change. Upon melting heat is transferred to the material, storing large amounts of heat at a constant temperature. Thermochemical energy storage (TCES) is produced when a chemical reaction with high energy involved in the reaction is used to store energy. TES technology is considered an effective system that can maximize the efficiency of heat pumps [11].

The temperature distribution of the thermal energy demands for individual end-uses can vary substantially. This study focused on a high-temperature heat pump (HTHP) cycle that can supply heat at approximately 200°C. The HTHP consists of a two-stage water vapor (R-718) Rankine cycle with intercooling (IC), and is expected to provide process heat at temperatures ranging from 100°C to 200°C. This temperature range is primarily required in the paper and printing industries and in other non-classified sectors [12]. Additionally, this study numerically evaluated and compared the performance of two different types of thermal energy storage systems, sensible and thermochemical energy storage, when connected to the HTHP.

2. Modeling of HTHP and TES systems

2.1. Multistage water vapor compression cycle

A two-stage water vapor compression cycle with intercooling was introduced as the HTHP cycle, Fig. 1. First, the working fluid, water/steam, is compressed to an intermediate pressure and then cooled close to its condensation temperature. The resulting slightly superheated steam is recompressed to the condensation pressure, which corresponds to the aimed condensing temperature. The International Association for the Properties of Water and Steam, based on the industrial formulation 1997 (IAPWS-IF97), was adopted to calculate the water/steam properties in the HTHP cycle.

The temperature of the heat source, T_{source}, which corresponds to waste heat, was fixed at 120°C. The evaporation and condensation temperatures, T_{evap} and T_{cond}, were set to 90°C and 160°C, respectively, with a temperature difference of ΔT_{lift} = 70 K. The intermediate pressure was determined to have the same pressure ratio between the first and second stages because the two-stage cycle showed the highest coefficient of performance (COP) when both compressors had the same pressure ratio in previous work. Additionally, all the temperature differences between the hot and cold sides after the heat exchangers were assumed to be 10 K ($T_{sup\ \&\ sub}$ = 10 K).

The heat sink flow, which flows through the intercooler and condenser, was designed to supply constant thermal energy to the TES system. It has the same pressure as the condenser, $P_{sink} = P_{cond}$, and the temperature of the sink inlet and outlet, $T_{sink\ in\ \&\ sink\ out}$, were fixed at 25°C and 200°C respectively. The amount of thermal energy obtained from the intercooler and condenser, $\dot{Q}_{sink}$, was determined to be 500 kW.

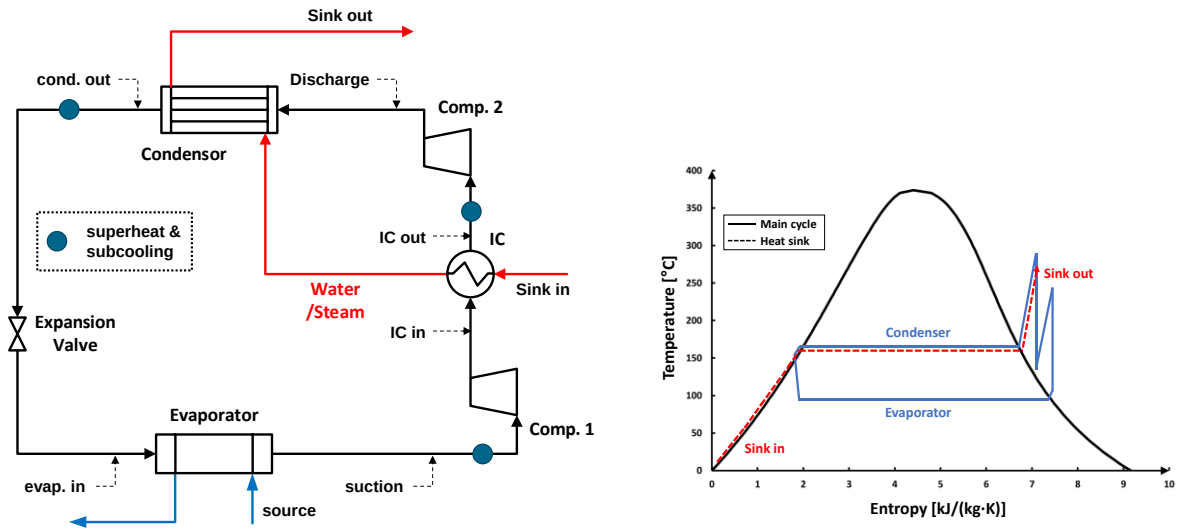

Fig. 1. Image of (left) schematic diagram of the HTHP cycle and (right) T-S diagram.

Table 1. Boundary conditions of HTHP and TES systems

Category	Item	Symbol	Value
HTHP cycle	Evaporation temperature	T_{evap}	90°C
	Condensation temperature	T_{cond}	160°C
	Superheat/Subcooling	$T_{sup\ \&\ sub}$	10 K
TES system	Power in storage mode	$\dot{Q}_{sink}$	500 kW
	Temperature in storage mode	$T_{sink\ out}$	200°C
	Pressure of heat sink	P_{sink}	$P_{sink} = P_{cond}$
	Mass flow rate of TES in discharge mode	m_{dis}	$m_{dis} = m_{stor}$

2.2. Thermal energy storage system

Sensible heat storage involves the use of a material to store thermal energy by increasing or decreasing the temperature of a storage medium. This energy storage method is widely used and is the most common type of TES technology. Many materials can be used for SHS materials such as water, air, oil, rock beds, brick, concrete, and so on. An SHS system using concrete is considered in this study. Concrete can withstand cyclic stress at temperatures of up to 500°C during numerous consecutive charging and discharging periods [13]. Therefore, concrete is suitable for storing sensible heat over long lifetimes.

The SHS system consists of two tanks: a hot tank containing concrete and a cold tank that stores air as a heat transfer fluid (HTF). The operating strategies are shown in Fig. 2. The low-temperature air, T_{amb} = 25°C, is heated by high-temperature steam in the HTHP cycle, T_{sink} = 200°C for 8 hrs, during storage mode, while high-temperature air transfers heat to low-temperature water/steam in the heat sink during the discharge mode. The state of water/steam in the heat sink flow was also calculated using IAPWS-IF97, and the performance of the SHS system was calculated based on the concrete properties at 200°C (Table 2) [14,15].

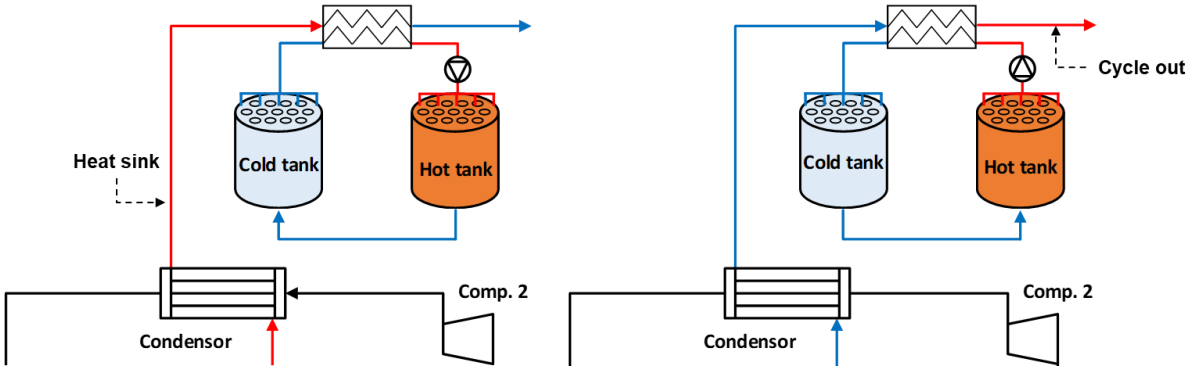

Fig. 2. Image of sensible heat storage system: (left) storage mode and (right) discharge mode.

Table 2. Properties of concrete for SHS systems

Temperature (°C)	Specific heat capacity, *Cp*, (J/(kg K))	Density, ρ, (kg/m^3)	Thermal conductivity, λ, (W/(m K))
100	832	2250	1.80
200	903	2250	1.60
300	1058	2250	1.40

Thermochemical energy storage (TCES) systems use reversible chemical reactions and have the advantages of a high storage density and long storage times without dissipation. Generally, reversible chemical reactions of TCES occur at high temperatures between the solid and gas phases. There are various types of chemical reactions for TCES, such as hydration, carbonation, and oxidation, and each reaction working pair has different working temperature and pressure characteristics. The strontium bromide and water ($SrBr_2/H_2O$) system was selected as the working pair for the TCES system in this study based on its promising performance at temperatures above 150°C [16,17]. The monohydrous $SrBr_2$ and $SrBr_2{\cdot}H_2O$ can store heat via dehydration, and the hydration of anhydrous $SrBr_2$ releases heat, as given in Eq. 1.

$$SrBr_2(s) + H_2O(g) \rightleftarrows SrBr_2 \cdot H_2O(s) \qquad \Delta H = 71.98\ \text{kJ/mol} \tag{1}$$

The operation of the TCES system with a packed bed reactor is shown in Fig. 3. During the heat storage mode, the dehydration of $SrBr_2{\cdot}H_2O$ is caused by a heat sink at 200°C, and the produced water vapor condenses in a water reservoir at 35°C, which is 10 K higher than the ambient temperature. The heat for the hydration, Q_{evap}, is assumed to use waste heat from industrial processes, in the same way as a heat source for the HTHP cycle, therefore, T_{hyd}, is lower than 110°C. Additionally, the molar mass, M, and density, ρ, of anhydrous and monohydrous $SrBr_2$ are shown in Table 3 [18].

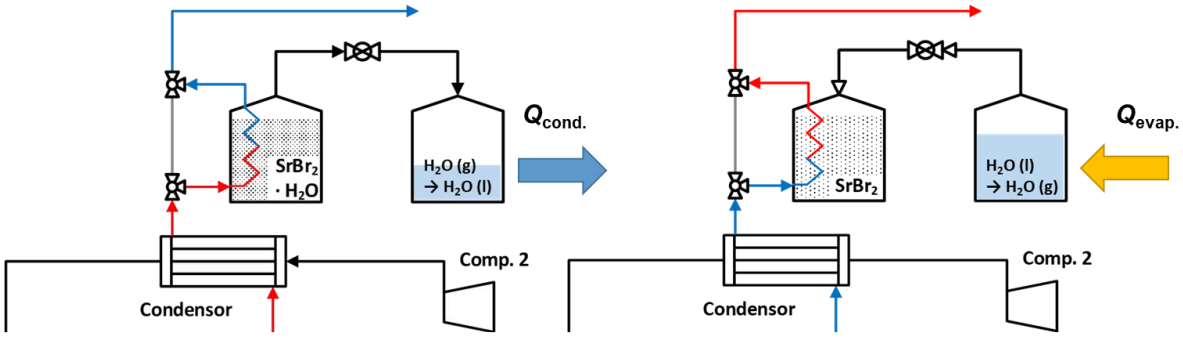

Fig. 3. Image of the thermochemical energy storage system: (left) storage mode and (right) discharge mode.

Table 3. Chemical and physical properties of $SrBr_2/H_2O$ TCES system

Material	Molar mass, M, (g/mol)	Density, ρ, (kg/m^3)	Enthalpy of hydration, ΔH, (kJ/mol)
$SrBr_2$	247.43	4216	71.98
$SrBr_2{\cdot}H_2O$	265.43	3911	

3. Methods and results

3.1. High-temperature heat pump cycle

The HTHP cycle operated at 90°C and 160°C for T_{evap} and T_{cond}, respectively, during storage for 8 hrs. It is assumed that the obtained thermal energy, 500 kW, is fully converted into a TES system, then 14400 MJ will be stored. The thermodynamic heat and energy balance of the multistage high-temperature heat pump cycle were estimated based on the IAPWS-IF97 standards. The intermediate pressure was defined from the suction and discharge pressures, with the assumption that each compression stage had the same pressure ratio. The overall thermodynamic properties, such as the pressure, temperature, and enthalpy, of each point of the HTHP cycle were determined. The important parameters are available from Eq. 2-3. Mass flowrate of the HTHP main cycle, $\dot{m}_{\text{main}}$, was induced as 0.19 kg/s, and the power consumption of two compressors, W_{comp}, was estimated to be 113.36 kW; the isentropic and mechanical efficiency, $\eta_{iso.}$ and $\eta_{mech.}$, are 0.78 and 0.90 respectively. From the obtained thermal energy from the condenser and IC, $\dot{Q}_{\text{sink}} = 500$ kW, and calculated W_{comp}, COP of the HTHP cycle was defined to 4.41, Eq. 4. Additionally, efficiency of the system was compared to that of an ideal cycle by introducing the thermodynamic efficiency, η_{carnot}, in Eq. 5 and 6. The Carnot efficiency, COP_{carnot},

represents the maximum energy efficiency of an ideal process that converts power to heat between two different temperatures, T_L and T_H [19]. The η_{carnot} value was calculated as 0.71.

$$\dot{m}_{main} = \frac{\dot{Q}_{sink}}{((H_{IC\,out} - H_{IC\,in}) - (H_{dis} - H_{cond\,out}))} \quad (2)$$

$$W_{comp} = \left(\frac{(H_{IC\,out} - H_{suc.}) \times \dot{m}_{main}}{\eta_{mech.}}\right) + \left(\frac{(H_{dis} - H_{IC\,out}) \times \dot{m}_{main}}{\eta_{mech.}}\right) \quad (3)$$

$$COP = \dot{Q}_{sink} / W_{comp} \quad (4)$$

$$\eta_{carnot} = \frac{COP}{COP_{Carnot}} \quad (5)$$

$$COP_{carnot} = \frac{T_H}{T_H - T_L} \quad (6)$$

According to the assumption in section 2.1, the mass flow rate of heat sink flow, $\dot{m}_{sink}$, has the same pressure as P_{dis} and it was calculated from the capacity of water/steam, c_p, and enthalpy, ΔH, of vaporization at 160°C, 2081.9 kJ/kg, Eq. 7. Because the c_p is variable by temperature, averaged specific heat capacities for the liquid and gaseous state, $\overline{c_p}_{liquid}$ and $\overline{c_p}_{gas}$, was adopted for the precise estimation. As a result, $\dot{m}_{sink}$ of the HTHP cycle is estimated to be 0.18 kg/s.

$$\dot{m}_{sink} = \frac{\dot{Q}_{sink}}{\left((T_{cond} - T_{sink\,in}) \times \overline{c_p}_{liquid} + (T_{sink\,out} - T_{cond}) \times \overline{c_p}_{gas} + \Delta H_{vap.,T_{cond}}\right)} \quad (7)$$

3.2. Sensible heat storage (SHS)

In storage mode, the HTHP cycle supplies 500 kW of heat for 8 hrs (τ_{stor} = 28800 s). Both TES systems stored thermal energy without any heat loss. The required concrete amounts for the SHS system can be calculated from Eqs. 8-9 based on material properties in Table 2, $m_{concrete} = 96647$ kg and $V_{concrete} = 43.0\ m^3$. As aforementioned in section 2.1, the temperature of the HTF in the TES was defined as 10 K lower than the heat sink out temperature, $T_{stor} = T_{sink\,out} - 10$ K, and the required airflow rate was obtained from Eq. 10, $\dot{m}_{air,stor} = 2.82$ kg/s.

$$m_{concrete} = \left(\dot{Q}_{sink} \times \tau_{stor}\right) / \left(c_{p_{concrete,200°C}} \times (T_{stor} - T_{amb})\right) \quad (8)$$

$$V_{concrete} = m_{concrete} / \rho_{concrete} \quad (9)$$

$$\dot{m}_{air-stor} = \dot{Q}_{sink} / \left(c_{p_{air,190°C}} \times (T_{stor} - T_{amb})\right) \quad (10)$$

On the discharge mode, the SHS system can have various cycle out temperatures, $T_{cycle\,out} < T_{stor} - 10$ K, by controlling heat output rate from the SHS system, $\dot{Q}_{SHS-dis}$. The required $\dot{Q}_{SHS-dis}$ According to the target $T_{cycle\,out}$ can be obtained from the enthalpy balance of heat sink flow and corresponding mass flowrate of air, $\dot{m}_{air-dis}$, on the SHS system are induced from Eq. 11. Additionally, the operation of the SHS system involves an air pump working, unlike the TCES system, for delivering the heat consecutively, Eq. 12. The values of differential the head, $h_{air\,pump}$, acceleration of gravity, g, and efficiency of the pump, $\eta_{air\,pump}$, are 20 m, 9.81 m/s^2, and 0.7 respectively. For what concerns the air mass flow rate, $\dot{m}_{air}$, and densities, ρ_{air}, is changed according to operation modes and conditions.

$$\dot{m}_{sink} \times \left(H_{T_{cycle\,out}} - H_{amb}\right) = \dot{Q}_{SHS-dis} = \dot{m}_{air-dis} \times \left(T_{stor} - T_{cycle\,out}\right) \quad (11)$$

$$W_{air\,pump} = \frac{(\dot{m}_{air} \times h_{air\,pump} \times g \times \rho_{air})}{\eta_{air\,pump}} \quad (12)$$

While the SHS system constantly consumes 3522.77 W for air pump work on storage mode, $\dot{Q}_{SHS-dis}$ and $W_{air\,pump-dis}$ are changed on discharge mode by target cycle out temperature, Fig. 4. Because heat sink flows have the same pressure to discharge pressure, P_{dis}, of HTHP main cycle, it has the same evaporation temperature of 160°C, and mass flow rate, $\dot{m}_{air-dis}$, is increased drastically to satisfy the increase $\dot{Q}_{SHS-dis}$ over the evaporation temperature. It was also found that the power consumption of the air pump increased consistently despite the heat output rate from the SHS system becoming stabilized over 160°C;

$\dot{m}_{\mathrm{air-dis}}$ increased from 22.8 kg/s to 45.9 kg/s on 170°C to 180°C of $T_{\mathrm{cycle\ out}}$ while $\dot{Q}_{\mathrm{SHS-dis}}$ shows stable values 487.45 kW and 497.68 kW.

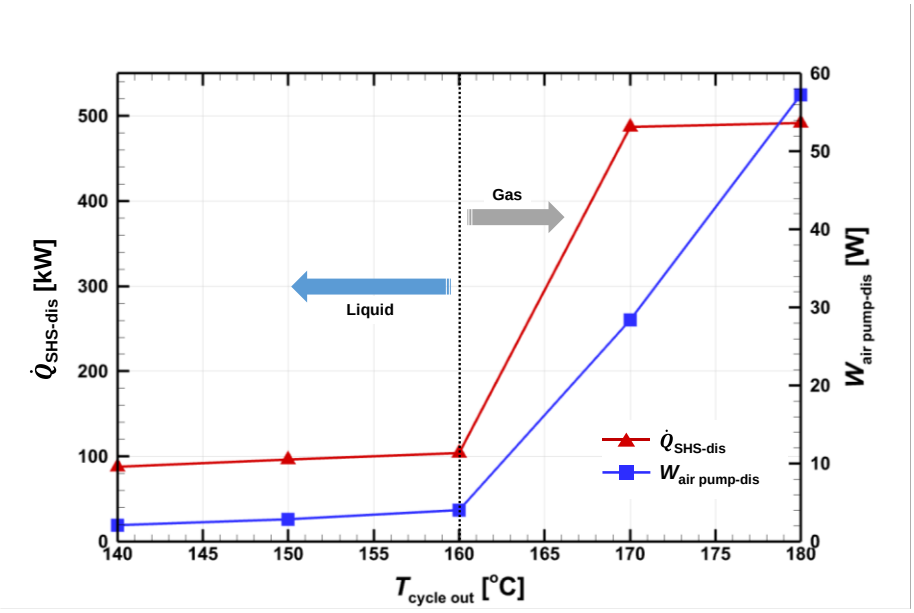

Fig. 4. Change of $\dot{Q}_{\mathrm{SHS-dis}}$ and $W_{\mathrm{air\ pump-dis}}$ by cycle out temperature on discharge mode.

3.3. Thermochemical energy storage (TCES)

The Gibbs free energy change of a reaction, ΔG, is obtained from the reaction enthalpy change, ΔH, and the entropy change, ΔS, as shown in Eq. 13.

$$\Delta G = \Delta H - T\Delta S \tag{13}$$

where ΔG has the following relationship with the reaction equilibrium constant, K_{eq}, for the gas-solid reaction assuming ideal gas properties Eq. 14. The reversible reaction condition is established at around $K_{\mathrm{eq}} = 1$ and the linear form of the Van't Hoff plot is obtained.

$$\ln K_{\mathrm{eq}}(T,P) = \ln\left(\frac{P}{P^0}\right) = \frac{\Delta G}{\mathrm{R}T} = -\frac{\Delta H}{\mathrm{R}T} + \frac{\Delta S}{\mathrm{R}} \tag{14}$$

From the reaction enthalpy, ΔH, molecular mass and density of $SrBr_2{\cdot}H_2O$, $M_{SrBr_2\cdot H_2O}$ and $\rho_{SrBr_2\cdot H_2O}$, in Table 3, the necessary amounts of $SrBr_2{\cdot}H_2O$ for the storage mode can be estimated as a mass, $m_{SrBr_2\cdot H_2O}$, of 53101 kg and volume, $V_{SrBr_2\cdot H_2O}$, of 13.6 m^3 from Eqs. 15-16, in terms of anhydrous $SrBr_2$, 49500 kg and 11.7 m^3.

$$m_{SrBr_2\cdot H_2O} = \left(\left(\frac{\dot{Q}_{\mathrm{sink}}}{\Delta H}\right)/M_{SrBr_2\cdot H_2O}\right) \times \tau_{\mathrm{stor}} \tag{15}$$

$$V_{SrBr_2\cdot H_2O} = m_{SrBr_2\cdot H_2O}/\rho_{SrBr_2\cdot H_2O} \tag{16}$$

Fig. 5 shows the Van't Hoff diagram of $SrBr_2/H_2O$ solid-gas reaction, ΔH = 71.98 kJ/mol and ΔS = 143.93 J/(mol·K) given in the NBS table. This TCES system possible to store heat by the accomplishment of dehydration at a certain temperature, T_{dehyd}, and achieve a higher output temperature than dehydration temperature, $T_{\mathrm{hyd}} > T_{\mathrm{dehyd}}$, particularly, since T_{hyd} is controllable from hydration pressure. Therefore, the discharge mode of the TCES system is also known as the temperature upgrade operation of a chemical heat pump [20].

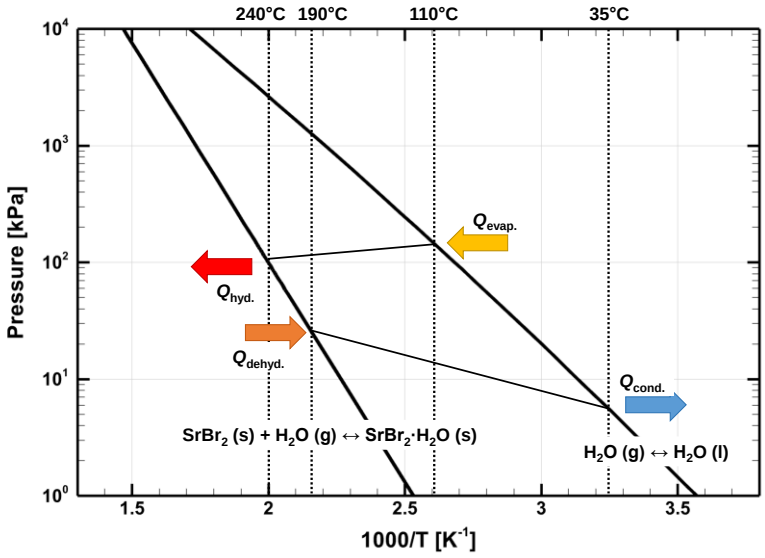

Fig. 5. Van't Hoff plot of $SrBr_2/H_2O$ solid gas-reaction.

In this study, during the heat storage operation, monohydrous $SrBr_2$, $SrBr_2 \cdot H_2O$, was decomposed at 190°C, 10 K lower than T_{sink}, and the produced water vapor was condensed at 35°C, 10 K higher than T_{amb}. Because it was assumed that waste heat from the industrial process was used for evaporation, the temperature for evaporation, T_{evap}, was limited to 110°C. Four different evaporation temperatures were selected, T_{evap} = 80°C, 90°C, 100°C, and 110°C, and hydration temperatures, T_{hyd} = 206°C, 217°C, 227°C, and 238°C, were obtained from the corresponding saturated water vapor pressures of 47.4 kPa, 70.2 kPa, 101.4 kPa, and 143.4 kPa. The heat output rate of the TCES system, $\dot{Q}_{\mathrm{TCES-dis}}$, is obtained from the first half of Eq. 9, and Table 4 shows the cycle out temperature, $T_{\text{cycle out}}$, operable discharge time, τ_{dis}, and $\dot{Q}_{\mathrm{TCES-dis}}$ by evaporation temperature, T_{evap}.

Table 4. Performance of TCES system on discharge mode

Evaporation temperature, T_{evap}, (°C)	Hydration temperature, T_{hyd} (°C)	Operable time, τ_{dis}, (hr)	Heat output rate of TCES, $\dot{Q}_{\mathrm{TCES-dis}}$, (kW)
80	206	8.03	498
90	217	7.96	502
100	227	7.90	506
110	238	7.83	510

3.4. Comparison of both TES systems

The heat output rate and operable discharge time of both the TES systems are compared in Fig. 6. Generally, the TCES system has a higher heat output rate, $\dot{Q}_{\mathrm{dis}}$, and cycle out temperature, $T_{\text{cycle out}}$, than the SHS system. SHS system has a maximum cycle output temperature, $T_{\text{cycle out}}$, of 180°C because the stored temperature, $T_{sotr.}$, is 190°C, however, the $T_{\text{cycle out}}$ of the TCES system obtained from equilibrium pressure on Eq. 12 is higher than 200°C. Additionally, the $T_{\text{cycle out}}$ of the SHS TES system has been decreased rapidly for below 160°C of $T_{\text{cycle out}}$, since the saturation pressure of the heat sink is assumed to have the same condensation temperature as with HTHP main cycle.

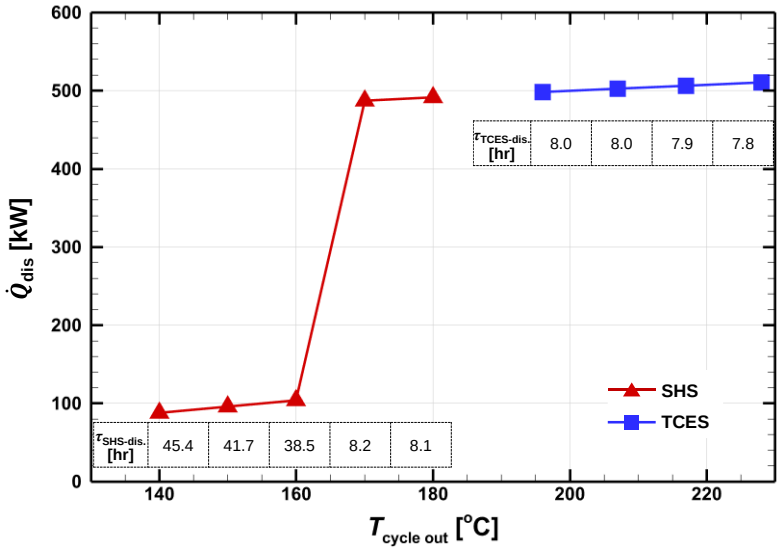

Fig. 6. Comparison of $\dot{Q}_{dis}$ and τ_{dis} in function of the cycle out temperature.

The round-trip efficiency (RTE) of the thermal energy storage system is expressed as the ratio of the energy output to the energy input, as shown in Eq. 17; the power consumption of the air pump, $W_{air\ pump}$, is considered only for the SHS system.

$$\eta_{RTE} = \frac{(\dot{Q}_{dis} - W_{air\ pump-\ dis}) \times \tau_{dis}}{(\dot{Q}_{sink} + W_{comp} + W_{air\ pump-stor}) \times \tau_{stor}} \quad (17)$$

On the RTE, on the other hand, the TCES system has a constant value, 0.82, since the TCES system can be utilizing waste heat from industrial processes for evaporating, Q_{evap}, without additional mechanical power, the RTE of SHS are decreasing from 0.79 to 0.72 with increasing heat output rate. Dramatically increased air mass flow rate on discharge mode, $\dot{m}_{air-dis}$, brings low RTE of SHS system at high cycle out temperature, $T_{cycle\ out}$, and heat output rate, $\dot{Q}_{dis}$. Compared to the concrete SHS system, $SrBr_2/H_2O$ TCES system only requires 45% and 68% less amount of mass and volume for storage; the TCES system also has 4-14% higher round-trip efficiency, Table 5.

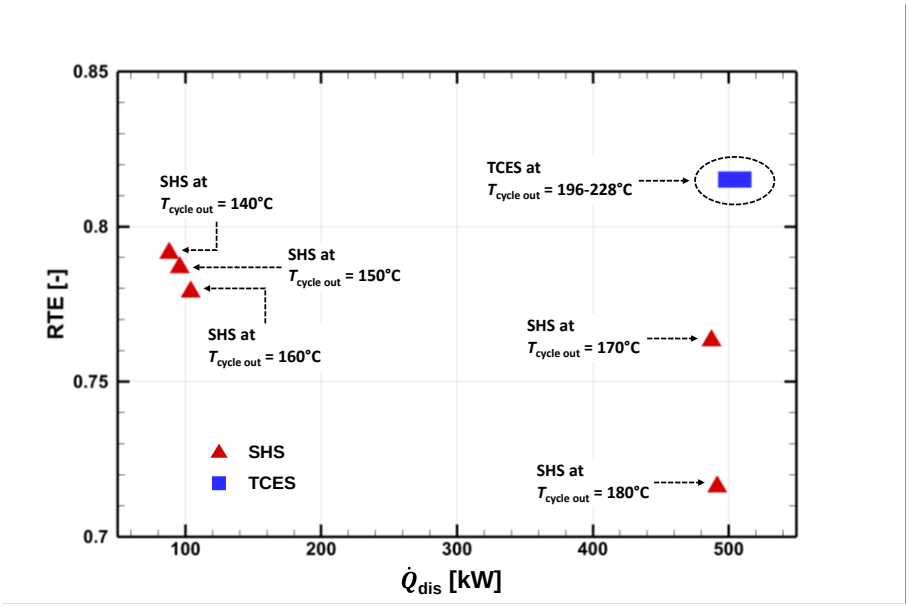

Fig. 7. Comparison of RTE according to heat output rate in the discharge mode.

Table 5. Specifications of TES systems

	SHS	TCES	Note
Material	Concrete	$SrBr_2 \cdot H_2O$ ($SrBr_2$)	TCES/SHS
Weight, *m*, (kg)	96647	53101 (49500)	0.55 (0.51)
Volume, *V*, (m^3)	43.0	13.6 (11.7)	0.32 (0.27)
RTE (-)	0.72-0.79	0.82	1.04-1.14

4. Conclusion

The performances of a multistage high-temperature heat pump (HTHP) and two different thermal energy storage (TES) systems connected to the HTHP cycle were investigated. The HTHP cycle had temperatures of 90°C and 160°C for the evaporator and condenser, respectively, and its performance was analyzed using a thermodynamic enthalpy balance. It was assumed that the HTHP cycle would supply 200°C and 500 kW of thermal energy for 8 hours during storage operation. The heat sink flow transferring thermal energy to the TES system is constrained to have the same pressure as the discharge pressure of the HTHP main cycle, $P_{\text{sink}} = P_{\text{dis}}$, and a constant flow rate, $\dot{m}_{\text{sink}}$.

The thermochemical energy storage system (TCES) has a higher discharge temperature and heat output rate, >200°C and ~500 kW, compared to the sensible heat storage (SHS) system. This is because the $SrBr_2/H_2O$ TCES system release higher temperature than assumed waste heat by considering the equilibrium pressure, whereas the SHS system does not allow for an upgrade in temperature. In particular, the heat output rate of the SHS system was significantly reduced when the cycle out temperature was lower than the condensation temperature, $T_{\text{cycle out}} < T_{\text{cond}}$. In terms of physical requirements, The TCES system has 45% and 68% lower material weight and volume requirements than the SHS system, and its round-trip efficiency is also higher because of the reduced power consumption of the air pump. These results confirmed the advantages of the TCES system for high-temperature thermal energy.

This approach will not only aid in the development of efficient HTHP and TES integration systems but also their effective development. Further study is possible through a detailed analysis of the HTHP cycle with various temperature ranges and different TES system configurations.

References

[1] Lamb WF, Wiedmann T, Pongratz J, Andrew R, Crippa M, Olivier JGJ et al. A review of trends and drivers of greenhouse gas emissions by sector from 1990 to 2018. Environ. Res. Lett. 2021;**16**(7):73005.

[2] Edenhofer O (ed.). Climate change 2014: Mitigation of climate change Working Group III contribution to the fiths assessment report of the intergovernmental panel on climate change.

[3] IEA. Key World Energy Statistics 2021; 2021.

[4] Huang F, Zheng J, Baleynaud JM, Lu J. Heat recovery potentials and technologies in industrial zones. *J Energy Inst* 2017;**90**(6):951-61.

[5] Brueckner S, Miró L, Cabeza LF, Pehnt M, Laevemann E. Methods to estimate the industrial waste heat potential of regions – A categorization and literature review. Renewable Sustainable Energy Rev. 2014;**38**:164–71.

[6] Chamoun M, Rulliere R, Haberschill P, Peureux J-L. Experimental and numerical investigations of a new high temperature heat pump for industrial heat recovery using water as refrigerant. *Ing J Refrig* 2014;**44**:177–88.

[7] German Energy Agency (DENA). Process heat in industry and commerce: Technology solutions for waste heat utilisation and renewable provision; 2016.

[8] van de Bor DM, Infante Ferreira CA. Quick selection of industrial heat pump types including the impact of thermodynamic losses. *Energy* 2013;**53**:312–22.

[9] Arpagaus C, Bless F, Uhlmann M, Schiffmann J, Bertsch SS. High temperature heat pumps: Market overview, state of the art, research status, refrigerants, and application potentials. *Energy* 2018;**152**:985–1010.

[10] Miró L, Gasia J, Cabeza LF. Thermal energy storage (TES) for industrial waste heat (IWH) recovery: A review. *Appl. Energy* 2016;**197**:284-301.

[11] Osterman E, Stritih U. Review on compression heat pump systems with thermal energy storage for heating and cooling of buildings. *J Energy Storage* 2021;**39**:102569.

[12] Fleitern Tobias, Jan Steinbach, Mario Ragwitz, Andreas Müller, Lukas Kranzl, Marcus Hummel et al. Mapping and analyses of the current and future (2020-2030) heating/cooling fuel deployment (fossil/renewables) Work package 1: Final energy consumption for the year 2012 Final report: 54296; 2016.

[13] Laing D, Lehmann D, Fiß M, Bahl C. Test Results of Concrete Thermal Energy Storage for Parabolic Trough Power Plants. *J Sol Energy Eng* 2009;**131**(4): 041007.

[14] Pan J, Zou R, Jin F. Experimental Study on Specific Heat of Concrete at High Temperatures and Its Influence on Thermal Energy Storage. *Energies* 2017;**10**:33.

[15] Anderberg Y, Forsén NE, Hietanen T, Izquierdo JM, A Le Duff, E Richter, RT Whittle, H Bossenmayer, HU Litzner, J Kruppa. Background documents to EN 1992-1-2 Eurocode 2: Design of concrete structures, Part 1-2: General rules - Structural fire design. Brussels, European Committee for Standardization; 2004.

[16] Richter M, Habermann EM, Siebecke E, Linder M. A systematic screening of salt hydrates as materials for a thermochemical heat transformer. *Thermochim. Acta* 2018;**659**:136-50.

[17] Stengler J, Bürger I, Linder M. Thermodynamic and kinetic investigations of the $SrBr_2$ hydration and dehydration reactions for thermochemical energy storage and heat transformation. *Appl. Energy* 2020;**277**:115432.

[18] Perry Dale L, *Handbook of Inorganic Compounds*. 2nd ed. Boca Raton: CRC Press; 2011.

[19] Jan Szargut. Component efficiencies of a vapour-compression heat pump. *Exergy, An International Journal* 2002;**2**(2):99–104

[20] Zamengo M, Yoshida K, Morikawa J. Numerical evaluation of a Carnot battery system comprising a chemical heat storage/pump and a Brayton cycle. *J Energy Storage* 2021;**41**:102955.